AIP | Review of Scientific Instruments

Optofluidic cell manipulation for a biological microbeam

Michael Grad, Alan W. Bigelow, Guy Garty, Daniel Attinger, and David J. Brenner

Citation: Review of Scientific Instruments **84**, 014301 (2013); doi: 10.1063/1.4774043
View online: http://dx.doi.org/10.1063/1.4774043
View Table of Contents: http://scitation.aip.org/content/aip/journal/rsi/84/1?ver=pdfcov
Published by the AIP Publishing

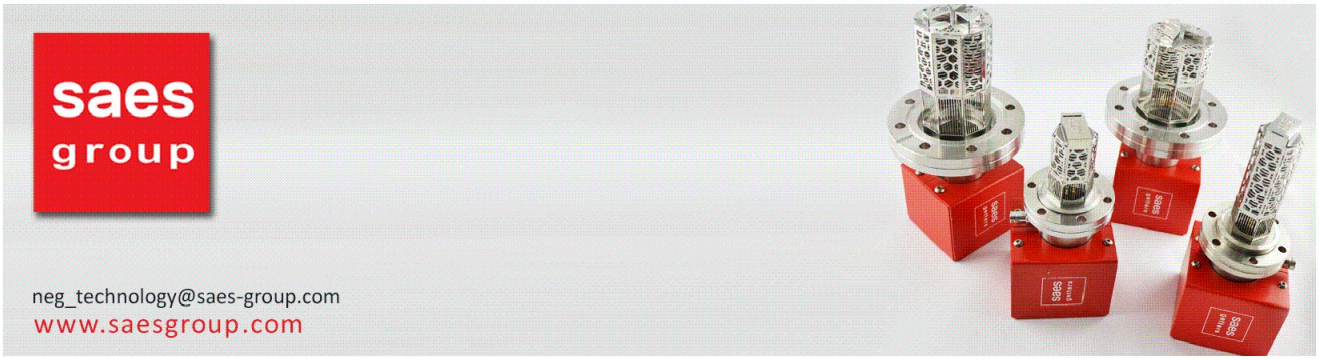

Optofluidic cell manipulation for a biological microbeam

Michael Grad,[1,2,a] Alan W. Bigelow,[2] Guy Garty,[2] Daniel Attinger,[3] and David J. Brenner[2]
[1]*Department of Mechanical Engineering, Columbia University, New York, New York 10027, USA*
[2]*Radiological Research Accelerator Facility, Columbia University, Irvington, New York 10533, USA*
[3]*Department of Mechanical Engineering, Iowa State University, Ames, Iowa 50011, USA*

(Received 16 October 2012; accepted 11 December 2012; published online 14 January 2013)

This paper describes the fabrication and integration of light-induced dielectrophoresis for cellular manipulation in biological microbeams. An optoelectronic tweezers (OET) cellular manipulation platform was designed, fabricated, and tested at Columbia University's Radiological Research Accelerator Facility (RARAF). The platform involves a light induced dielectrophoretic surface and a microfluidic chamber with channels for easy input and output of cells. The electrical conductivity of the particle-laden medium was optimized to maximize the dielectrophoretic force. To experimentally validate the operation of the OET device, we demonstrate UV-microspot irradiation of cells containing green fluorescent protein (GFP) tagged DNA single-strand break repair protein, targeted in suspension. We demonstrate the optofluidic control of single cells and groups of cells before, during, and after irradiation. The integration of optofluidic cellular manipulation into a biological microbeam enhances the facility's ability to handle non-adherent cells such as lymphocytes. To the best of our knowledge, this is the first time that OET cell handling is successfully implemented in a biological microbeam. © *2013 American Institute of Physics*. [http://dx.doi.org/10.1063/1.4774043]

I. INTRODUCTION

A biological microbeam has the ability to deliver precise doses of radiation to single cells.[1] The use of microbeams has led to major advances in assessing intra- or inter-cellular biological responses to radiation, such as DNA damage in subnuclear targets (e.g., single or double strand DNA breaks),[2] or bystander responses.[3] The Radiological Research Accelerator Facility (RARAF) at Columbia University was one of the first facilities with a microbeam for radiation-biology applications.[4] Today there are over 30 biological microbeams in the world.[1] Until recently, most of the microbeam development at RARAF has been on particle beam size,[5] microbeam type,[6] or improved imaging techniques.[5] Current cell handling at RARAF is mostly for adherent cells,[7] and this paper describes a new paradigm in cell handling through the integration of an optofluidic cellular manipulation platform with a biological microbeam endstation.

A typical biological microbeam experiment at RARAF involves cells plated on a dish, with cell targeting enabled by moving the dish to the microbeam using a computer-controlled stage. This experimental setup is ideal for adherent target samples, such as fibroblasts. Recently, RARAF has introduced a microfluidic channel meant to bring a continuous flow of cells to the microbeam radiation source, using flow and shoot technology (FAST).[7] This technology enables the handling of non-adherent cells (e.g., lymphocytes), as well as increases the throughput of cellular irradiation nearly tenfold. However, the system is designed for large numbers of cells, and the fixed flow pattern is unidirectional (from inlet to outlet) and at constant velocity. To attain the flexibility of a reconfigurable system, RARAF is pursuing a dynamic optofluidic cellular manipulation platform for experiments that require the flexibility to precisely place a cell at any location on a two-dimensional surface.

Recently, optofluidic manipulation techniques have been considered in biological irradiators, because of the ability to use light beams to remotely handle particles: optical tweezers have been used to manipulate oocytes in a laser microsurgery device,[8] and optical tweezers have been integrated into a synchrotron radiation probe.[9] Optical tweezers use the radiation pressure from a focused laser to trap particles using two forces: a scattering force (in the direction of the beam) and a gradient force caused by refraction (normal to the laser beam, towards its center).[10] Instead of using optical forces to directly trap cells, optoelectronic tweezers (OET) use light to activate photoconductive surfaces and indirectly trap cells using dielectrophoresis, a phenomenon that requires five orders of magnitude less light than optical tweezers.[11] Since the first publication on OET in 2005,[11] optofluidic manipulation techniques have received an enormous amount of attention. A full review of existing optoelectrofluidic applications and platforms can be found in existing literature.[12] Briefly, optoelectrofluidic devices have been demonstrated to dynamically manipulate a range of biological and non-biological materials, including polymer beads and several types of cells,[13,14] nanoparticles,[15] and multiphase droplets.[16,17] Numerical models of OET devices have also been presented to model the electric field in the device,[18] and build upon the electric field with a molecular dynamics simulation.[19] To date, no OET devices have been used to control cells in a microbeam irradiator.

Section I A of this paper will present the background theory behind the operation of OET devices that will be introduced into the microbeam irradiator. Section II presents the design and optimization of the devices. Section III describes the materials and methods used to fabricate the devices, as

[a]Author to whom correspondence should be addressed. Electronic mail: mg2705@columbia.edu.

well as the specificities of the laser microbeam system. Finally, Sec. IV demonstrates our ability to manipulate beads and cells, and irradiate cells using a laser irradiator based on multiphoton excitation.

A. Light-induced DEP theory

In the presence of an alternating current(ac) electric field, the internal charges in a polarizable dielectric particle will migrate into an induced dipole, and each pole will experience a force from the electric field ($F = qE$). If the ac field is spatially non-uniform, the force on one pole will dominate over the other, resulting in a body force on the particle; this phenomenon is called dielectrophoresis (DEP). The force can be positive or negative, and is given by[20]

$$F_{\mathrm{DEP}} = 2\pi r^3 \varepsilon_m \mathrm{Re}[f_{cm}(\omega)]\nabla(E^2), \tag{1}$$

where r is the particle radius, ε_m is the permittivity of the medium, and $\nabla(E^2)$ is the gradient of the square of the magnitude of the electric field. $\mathrm{Re}[f_{\mathrm{cm}}(\omega)]$ is the real part of the Clausius-Mossotti factor, where $\mathrm{Re}[f_{\mathrm{cm}}(\omega)] = \frac{\varepsilon_p^* - \varepsilon_m^*}{\varepsilon_p^* + 2\varepsilon_m^*}$, and $\varepsilon_i^* = \varepsilon_i - j\frac{\sigma_i}{\omega}$. In these expressions, ε_i is the permittivity of the particle or medium, σ_i is the conductivity of the particle or medium, and ω is the angular frequency of the electric field. All other terms are positive, so the sign of the Clausius-Mossotti factor determines the direction of the applied force. This factor can be influenced by the type of medium, the material, and size of the particle, as well as the frequency of the electric field.[20]

A DEP trap is typically created using fixed metallic electrodes.[21,22] Another technique is to create dynamic virtual electrodes for a reconfigurable geometry.[23] When a photoconductive coating is patterned on a planar electrode, the projection of visible light onto the surface increases the local conductivity by an order of magnitude; as a result, a virtual electrode is created. This dynamic virtual electrode can be used to create a moving DEP trap and manipulate particles to any location on the surface. That design and concept is referred to as optoelectronic tweezers (OET).[23]

Typical OET devices include two ITO covered glass slides, with projected light applied onto the photoconductive electrode from a direction akin to transmission illumination (i.e., from the opposite direction as the microscope visualization).[23] Since the RARAF microbeam irradiator comprises an epi-illumination microscope atop the exit portal of a vertical ion-beam line, patterned light projection and microscope visualization occur from the same side. Therefore, instead of using two transparent indium-tin oxide (ITO) electrodes, we only use one ITO electrode and one gold electrode. The gold surface can reflect any unabsorbed light back onto the photoconductive layer for further absorption. Also, typical OET devices are parallel plates separated by a double-sided tape spacer.[13,23] Instead, we built a microfluidic chamber with 1 inlet and 1 outlet port using a rubber gasket and a customized plastic clamp. Figure 1 depicts the cross section of an OET device. Further detail into the fabrication of the OET surfaces and the microfluidic chamber is described in Sec. III A.

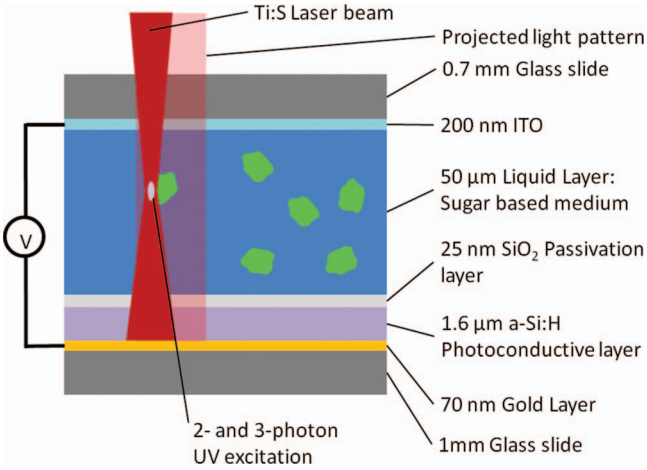

FIG. 1. Cross section schematic of an optofluidic manipulation device. The projected pattern and the microscope visualization both come from the top surface, so the bottom electrode does not need to be transparent.

II. DESIGN

A 2D static numerical simulation using the root-mean-square (RMS) voltage, or the quadratic mean of the ac voltage, can predict the force on particles, similar to previously published work.[18] Figure 2 shows the geometry of the simulation of a DEP trap created by the virtual electrodes in an OET device, and the colors and arrows represent the magnitude and direction of the gradient of the electric field. The electrical boundary conditions include electric insulation on the side walls, the applied RMS voltage ($V_0 = 10$ V) on the top edge, and ground on the bottom edge. The conductivity of the bottom edge is set to the light and dark conductivities of amorphous silicon, or 6.4e-5 S/m and 6.6e-6 S/m, respectively.[18] A commercial finite element software package (COMSOL Multiphysics 4.3) was used to perform the calculations of the electric field in the OET device and the DEP forces.

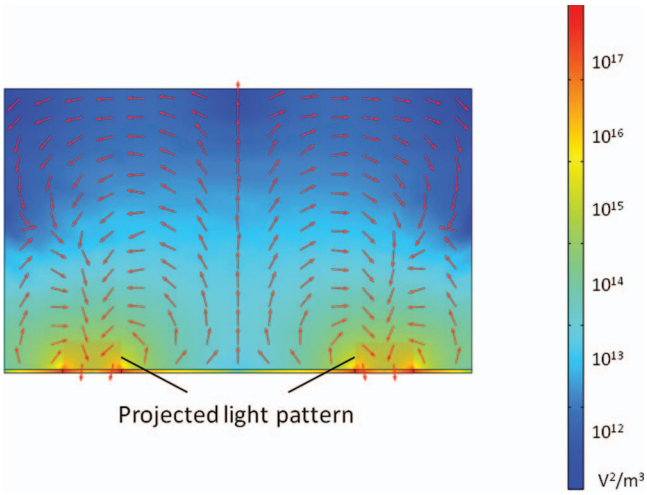

FIG. 2. Geometry of 2D numerical simulation. The colors represent the logarithmic plot of the gradient of the square of the electric field magnitude, and the arrows represent the direction of the DEP force on a particle attracted to the light pattern. The magnitude of the DEP force is calculated using Eq. (1).

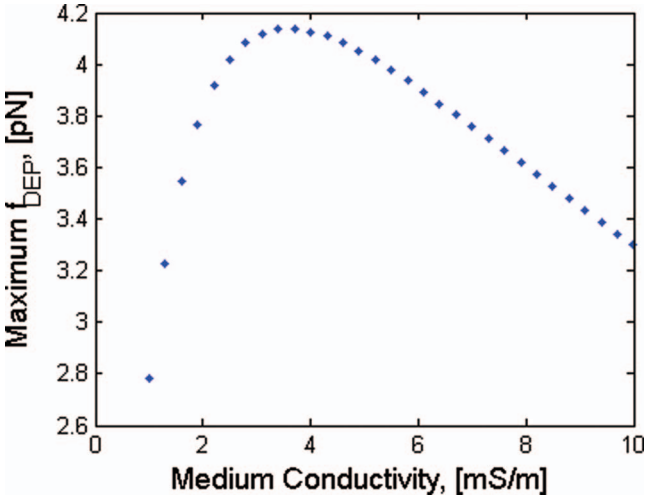

FIG. 3. Simulated force as a function of medium conductivity. The RMS voltage applied is 10 V, at a frequency of 100 kHz. The maximum force occurs at around 3-4 mS/m.

The DEP force is calculated using Eq. (1). The parameters for particle and medium permittivity and conductivity were taken from previously published work:[18] the relative permittivity of the medium is 78; the relative permittivity of particle is 2.5; and the electrical conductivity for the particle consists of the bulk conductivity (σ_{bulk} = 1e-16 S/m) and surface conductivity (K_s = 2e-9 S/m), where $\sigma = \sigma_{bulk} + 2K_s/radius$,[18] and is equal to 4e-4 S/m. The electrical conductivity of the medium is varied between 1 and 10 mS/m, and the resulting DEP force on a 10 μm bead is shown in Figure 3.

The maximum force applied on the particle is ~4 pN, which is on the order of published values of 1-10 pN.[13] This maximum force occurs at around 3-4 mS/m, and we have set the conductivity of the solutions used in the experimental validation (Sec. IV A) according to these values.

III. MATERIALS AND METHODS

A. Fabrication

The light-induced DEP device was manufactured in the Center for Engineering and Physical Science Research (CEPSR) Clean Room at Columbia University. The photoconductive surface was fabricated on a standard microscope slide as follows: 70 nm of gold was thermally evaporated onto the glass slide (Edwards/BOC Resistive Thermal Evaporator, Sanborn, NY, USA). A plasma enhanced chemical vapor deposition tool (Oxford PlasmaPro NPG80 PECVD, Concord, MA, USA) was used to deposit a 1.6 μm thick layer of hydrogenated amorphous silicon (a-Si:H) using a cover slip as a shadow mask for electrical connections to the gold layer. Deposition parameters are 350 sccm SiH_4, 25 sccm H_2, 1000 mTorr, 300 °C, and 30W RF power for 60 min. The same tool was used to deposit a 25 nm thick SiO_2 layer on top of the amorphous silicon to act as a passivation layer, with deposition parameters including 180 sccm SiH_4, 710 sccm N_2O, 300 ° C, 1000 mTorr, and 20 W RF power for 30 s.

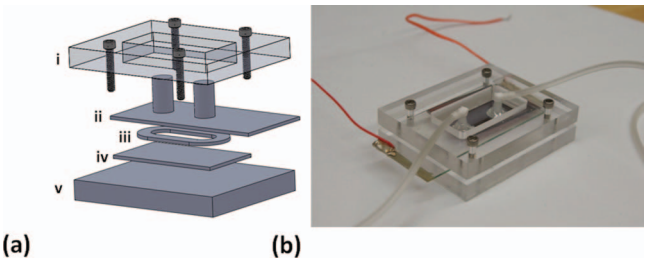

FIG. 4. (a) The microfluidic chamber consists of the OET sandwich (ii) and (iv) separated by a 50-μm thick rubber gasket (iii) and held together by a PMMA clamp and 4 screws (i) and (v). (b) Microfluidic connectors were glued around holes drilled into the top surface.

Commercial ITO-covered glass slides (Delta Technologies, Loveland, CO, USA) were used as the top electrode, because this surface must be transparent for the projected light pattern and irradiation laser to pass through it. Holes for the microfluidic connections were drilled into the top glass slide using a CNC desktop mill (Minitech Minimill 3, Atlanta, GA, USA) and diamond coated drill bits (McMaster-Carr, Robbinsville, NJ, USA). Ports were fixed to the top surface by gluing 1/16″ ferrules (Upchurch Scientific, Oak Harbor, WA, USA) around the drilled holes. A removable microfluidic connection and 1/16″. ID tubing was attached by plugging an elbow connector into each of these ports (Value Plastics, Fort Collins, CO, USA). Conductive epoxy was used to connect wires to the gold and ITO surfaces. The ac bias voltage is provided from a function generator (BK Precision 4070A, Yorba Linda, CA, USA) and a wideband amplifier (Krohn-Hite 7600M, Brockton, MA, USA).

The top and bottom surfaces were separated by a 50 μm rubber gasket and held together using a polymethylmethacrylate (PMMA) clamp and 4 screws. The clamp was milled from 1/4 in. PMMA slabs using the same CNC desktop mill described above, and the images in Figure 4 show the clamp and gasket setup. This closed system, including the tubing and syringe inlet/outlet, has the benefit of eliminating evaporation during longer experiments.

B. Integration into the RARAF microbeam

Geometrical constraints of the RARAF microbeam endstation prevent the integration of a platform that uses transmission illumination (i.e., from the opposite direction as the microscope visualization) to project the patterned light.[23] This is because the beam line protrudes from the bottom of the microscope, requiring that light sources must be introduced from the top side of the chip. There are three separate light sources that are all required for the experiment described below: the projected OET image generated by a commercial projector (Epson EMP-755, Nagano, Japan), a titanium sapphire (Ti:S) laser for cell irradiation (Coherent Chameleon, Santa Clara, CA, USA), and a mercury lamp to illuminate fluorescent cells (EXFO Acticure EFOS A4000, USA). The fluorescent light emitted from the cells must also be collected and delivered to an EMCCD camera (Princeton Instruments PhotonMax 512, Trenton, NJ, USA). Figure 5 shows: (1) the light paths at the

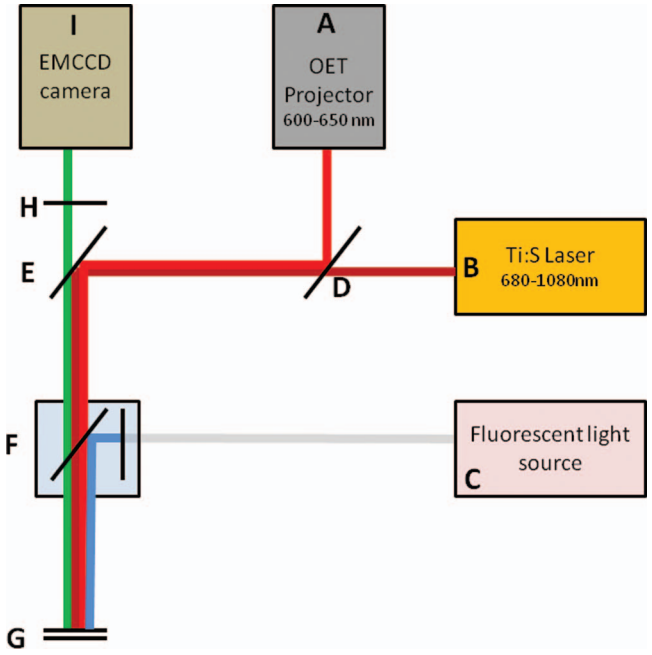

FIG. 5. The experimental setup and hardware required to integrate the 3 light sources (A), (B), and (C) into the microscope. Optical elements such as a cold mirror (D), dichroic mirror (E), and GFP cube (F) are used to project red and blue light onto the sample (G), and a green emission filter (H) only allows the signal from the stained/GFP-tagged cells to reach the camera.

microscope end station for the OET projected image and the Ti:S laser for UV irradiation through multiphoton excitation, and (2) the fluorescent imaging system.

The three light sources are labeled A, B, and C in Figure 5. The projected OET image is red (600-650 nm, and the Ti:S laser[1] is tunable to wavelengths between 680 nm and 1080 nm. These two light sources are combined to become co-axial by a cold mirror (Omega 63193, Stamford, CT, USA), labeled D in Figure 5, that allows wavelengths above 700 nm (e.g., the tuned laser) to pass through, and reflects wavelengths shorter than 700 nm (e.g., the projected image). Both these light sources are reflected down the microscope body by a long-pass red dichroic mirror (Chroma Technology Z680DCSP, Bellows Falls, VT, USA) that reflects wavelengths above 600 nm, labeled E in Figure 5.

The optical element labeled F in Figure 5 is a GFP cube (Chroma Technology ENDOW GFP HYQ Cube, Bellows Falls, VT, USA) with a blue 450 nm–490 nm bandpass excitation filter, a 500 nm long pass blue/green dichroic mirror, and the green emission filter removed. Removing the emission filter allows the red light sources A and B to pass through the cube to reach the sample. The mercury lamp/fluorescent light source, labeled C in Figure 5, is combined with the first two light sources by this cube to illuminate the green fluorescent cells.

After light from all three light sources are introduced to the sample (G), reflection and fluorescent signals return through the cube and dichroic mirror, and pass through one final element before reaching the EMCCD camera labeled I in Figure 5. The green band-pass emission filter (Chroma Technology 500/140, Bellows Falls, VT, USA) that was removed from the GFP cube is placed just beneath the camera to prevent the laser and projected image from overwhelming the CCD sensor, and labeled H in Figure 5. Ideally, only the green emission from the GFP tagged cells will reach the camera.

C. Cell and bead suspension preparation

In Sec. IV, we describe three sets of experiments. The first experiment uses polymer beads to validate OET and optimize OET control. The second experiment uses a fluorescently stained fibrosarcoma cell line (HT1080) to validate OET cell control. The third experiment validates the irradiation of the same type of fibrosarcoma cells, HT1080, modified by Chen to contain GFP tagged to a DNA single-strand break repair protein (XRCC1).[24]

The polymer bead solutions were prepared by washing and resuspending 10 μm microspheres (Molecular Probes F8890, Invitrogen/Life Technologies, Grand Island, NY, USA) in de-ionized (DI) water. The conductivity of the prepared suspension was altered using small amounts of KCl, and was verified using a hand-held conductivity meter (Omega CDH-5021, Stamford, CT, USA). Several solutions with different conductivity were prepared, as described in Sec. IV A.

The stained cell suspensions were prepared using a green cytoplasmic dye (Cell Tracker Green CMFDA, Invitrogen/Life Technologies, Grand Island, NY, USA). The staining procedure is as follows: the cells were incubated for 1 h in a solution of 6 μL stain and 4 mL cell medium. The cells were washed with PBS and trypsinized for 1 min, and resuspended in a low conductivity solution consisting of DI water, 8.5% sucrose, and 0.5% dextrose. The cells were rinsed by spinning at 300 rpm for 4 min and resuspending them in the same low-conductivity medium. The conductivity of the medium was measured to be $\sim$2 mS/m. The washing and resuspending procedures for the GFP-tagged cells in the third experiment is the same as described for the stained cells.

D. Projection software

The light pattern is generated by a projector connected to a computer. The displayed image can be created by any image production software, including a custom optical control software,[18] or commercial software such as Microsoft PowerPoint.[13] Custom software that is dedicated for convenient image manipulation can be more versatile and provide more control to the microbeam users, therefore a MATLAB program (code available in supplementary information[29]) was created to project a movable shape. The user can control the RGB color, translation, dilation, rotation, speed, and linewidth of the shape using simple keyboard commands. Figure 6 shows the output of the custom program.

The custom features offered by this software give complete control to the user. As described in Sec. III B, there is a green band-pass filter to prevent the red image from overwhelming the camera. Therefore, in order to see the location of the shape, the RGB values for the color can each be tuned separately, allowing a green shape to be projected for light to reach the camera set to smaller exposure times.

FIG. 6. Projected MATLAB image. The user can control the color, location, speed, and size of the shape using keyboard arrows and letters. The typical projected length scale is on the order of 10-100 μm after passing through the microscope objective.

IV. EXPERIMENTS TO VALIDATE OET AND LASER IRRADIATION

We verify the control and integration of the OET device in three experiments. First, we used green fluorescent beads suspended in a variety of liquid conductivities to validate the optimization performed in Sec. II, as discussed in Sec. IV A. Section IV B shows the handling of fluorescent stained cells to verify the operation of the OET device, and Sec. IV C shows the validation of the laser irradiator by the demonstration of DNA damage (nuclei focus formation) and of cell damage (laser ablation or lysis) of GFP-tagged cells.

A. Bead control

Initial tests were performed with polymer beads to validate the OET system. Figures 7 and videos 1 and 2 show the manipulation of polymer beads. In Figure 7, a single fluorescent bead trapped in an optically induced negative DEP trap,

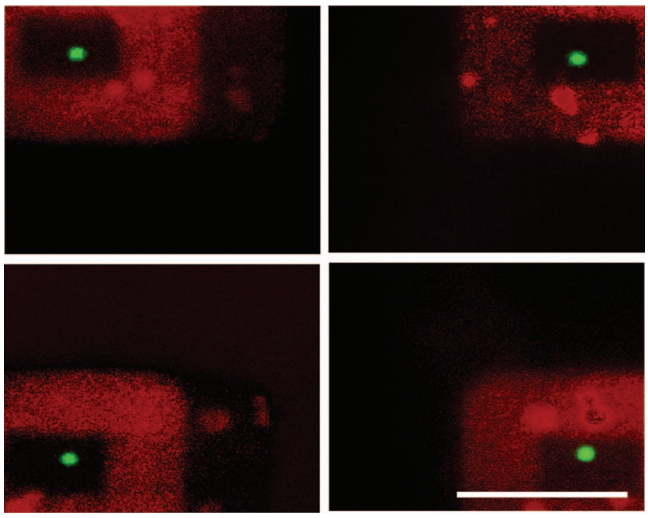

FIG. 7. Four images displaying the ability to move a single bead to each corner of the screen. The scale bar is 100 μm (enhanced online) [URL: http://dx.doi.org/10.1063/1.4774043.1]; [URL: http://dx.doi.org/10.1063/1.4774043.2].

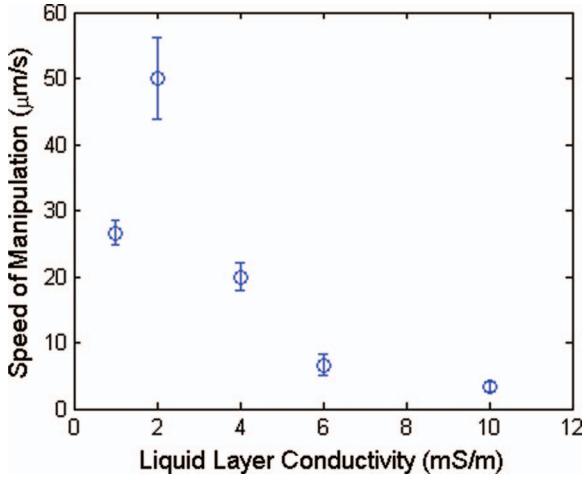

FIG. 8. Experimental speed of manipulation as a function of liquid layer conductivity. Polymer spheres with 10 μm diameter were manipulated by OET with 10 V and 100 kHz, reaching speeds of up to 50 μm/s.

and moved to the four corners of the screen. As mentioned in Sec. I A, the sign of the Clausius Mossotti factor determines whether the force from DEP is attractive or repulsive. The Clausius Mossotti factor of polymer beads is calculated to be negative at 100 kHz, therefore the bead within the pattern will be repelled from the light and trapped in the center of the square.

The trapped bead was moved around the screen at different speeds, which is controlled by setting the appropriate step size between refreshed images. The maximum speed of manipulation is determined by the maximum speed at which the shape can be moved before the bead can no longer remain trapped. Figure 8 shows the experimental maximum speed for different liquid conductivities.

The series of experiments represented in Figure 8 were performed with 10 μm diameter polystyrene beads suspended in DI water spiked with KCl to achieve different conductivities. The height of the chamber is 50 μm, and the voltage and frequency were 10 $V_{p\text{-}p}$, and 100 kHz. The speed of manipulation is directly proportional to the force that is applied on the particle. Therefore, we can infer that the maximum force is applied for conductivities around ~2 mS/m. The velocity of the particles is ~50 μm/s, and is in line with published values between 40 μm/s[13] and 105 μm/s[23].

B. Cell control

In this section we describe the control of fluorescently stained HT-1080 cells. The Clausius-Mossotti factor for these cells is positive, therefore the cells are attracted to the solid circle light pattern.[13] Figure 9 shows three frames taken from video 3 manipulating a single cell, with the cell placed at three different locations.

C. Cell irradiation: DNA damage and cell damage

The third experiment targeted XRCC1 GFP-tagged HT1080 cells with UV microspot radiation using the a multiphoton laser irradiator.[6] XRCC1 is a repair protein that is

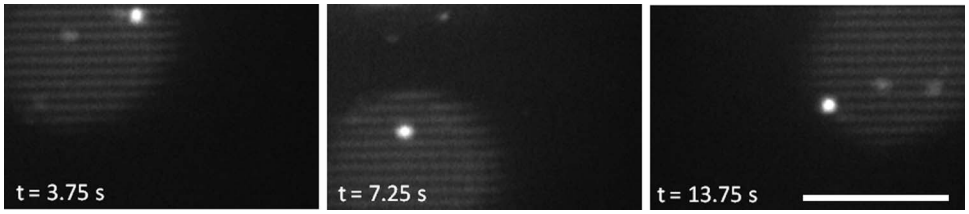

FIG. 9. Three frames taken from video 3 showing the ability to move a single fluorescent cell. The pattern is red with a small amount of green added for visibility through the green band pass filter. The cells are stained with cell tracker green cytoplasmic stain. The scale bar is 100 μm (enhanced online) [URL: http://dx.doi.org/10.1063/1.4774043.3].

recruited to single-strand DNA breaks.[24] Initially the entire cell nucleus is dimly fluorescing because the proteins are distributed throughout the nucleus. When the nucleus is irradiated, the repair proteins move toward the single-strand DNA breaks. This results in a localization of fluorescence into bright foci, visible by the EMCCD camera on the microbeam endstation. Figure 10 shows a time-lapse image sequence of a cell irradiation.

Because only the XRCC1 proteins in the nucleus are expressing GFP, the cells are not very bright. Our cooled EMCCD camera requires 500 ms exposure time and 4000 gain to adequately image the cells. However, we chose to use these cells because their response to site-specific radiation damage can be visualized in real time via localization of the repair protein as fluorescent foci.[24] These foci appear within 5-10 s and fade away after several minutes, consistent with the repair time of DNA single-strand breaks.

With such a long exposure time, any light from the projected pattern will saturate the camera's sensor. For this reason we included a green bandpass filter just before the camera, as described in Sec. III B. This filter blocks the red pattern while letting light from the green cells pass to the camera.

Above certain intensities, the use of lasers in biology has been shown to lyse, damage, or cause apoptosis-like cell death.[25–27] Figure 11 shows images of a cell being manipulated with OET and irradiated. The laser is positioned at the center of the image. The cell which starts on the left side of the screen (Figure 11(a)), is brought into position in the middle image for irradiation (Figure 11(b)). The cell is targeted with 28.95 mJ of UV radiation between frames B and C. The disappearance of the cell from Figure 11(c) and the dispersal of the fluorescent molecules is attributed to cell damage from radiation.[27]

V. DISCUSSION

The goal of this work was to integrate an optofluidic manipulation platform into RARAF's laser-based UV microspot irradiator, and demonstrate the successful operation of this device before, during, and after an irradiation. With the proper dichroic mirror and filter selections described in Sec. III B, we were able to successfully integrate the OET platform into the laser irradiator. Successful experiments and modeling of OET control of beads were demonstrated in Figs. 3 and 8. The numerical simulations in Sec. II predicted a peak in force at a conductivity of around 3-4 mS/m, and the experiments in Sec. IV A yielded a maximum velocity of 50 μm/s, occurring at 2-3 mS/m. These predicted forces and experimental velocities both match with previously published values. Figures 7–9, along with videos 1, 2, and 3, demonstrate our ability to control beads and cells. Figures 10 and 11 demonstrate successful irradiation of cells in suspension, yielding DNA damage and cell damage.

Future work will include the fabrication of an OET device with a thin bottom substrate for integration into the charged particle microbeams at RARAF. These microbeams

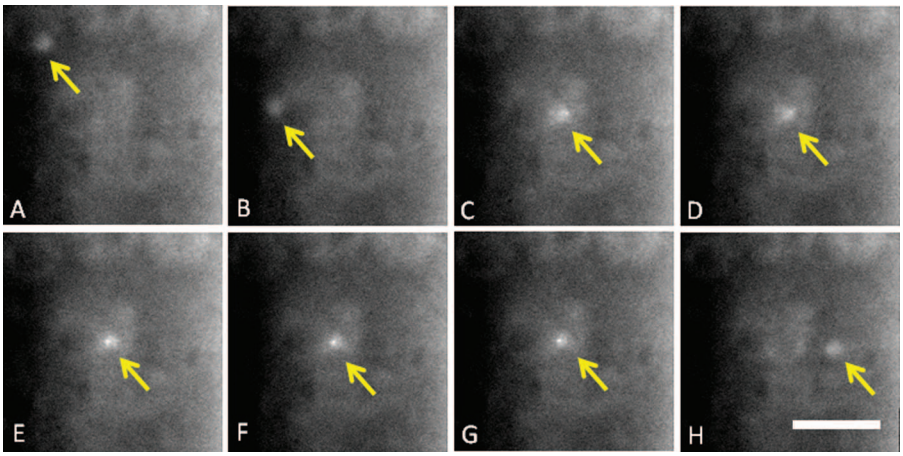

FIG. 10. With low exposures of radiation (3.6 mJ, 800 nm, which acts like 400 nm or 267 nm in a 2- or 3-photon excitation mode), single strand breaks are created in the nucleus. XRCC1 is a repair protein that moves towards the single strand breaks and forms a brighter fluorescent focus. The first seven frames depict images taken every 10 s. A cell starts in the top left corner of the screen (a), is brought to the center of the screen using OET for irradiation (b), and a focus is formed (c–g). Finally, after 5 min, the focus has faded and the cell is moved to the right side of the screen (h). Images are taken at 500 ms exposure time with the projected light pattern filtered out by a bandpass filter, and the scale bar is 100 um. Arrows are provided to guide the reader to the location of the cell.

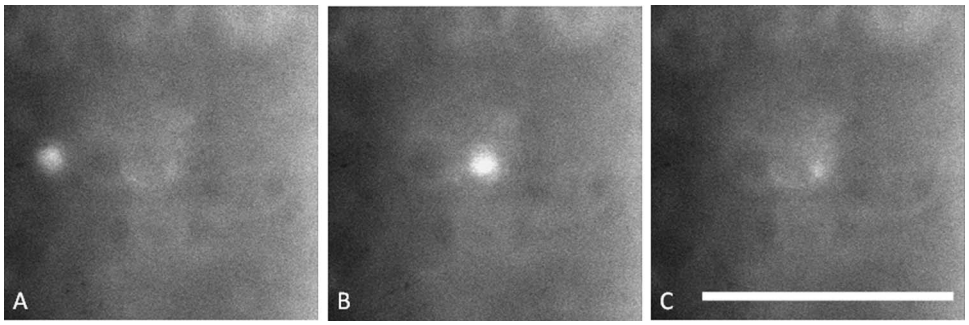

FIG. 11. With high exposures of UV radiation (28.95 mJ, 750 nm, which acts like 375 nm or 250 nm in a 2- or 3- photon excitation mode), the entire cell is damaged. The cell starts on the left side of the image (a), and is brought to the center of the middle image using OET (b) for irradiation (c). Images are taken at 500 ms exposure time with the pattern filtered out by a green bandpass filter, and the scale bar is 100 μm.

can target individual cells with alpha particles ($^4He^{++}$) and protons (H^+). However, the range of 5 MeV alpha particles in absorbing materials is limited to 25 μm in silicon, and this value inversely scales with the density of the material (e.g an ion passing through a material with twice the density will have half the range). Therefore, in order to use the OET device with the charged particle microbeam systems at RARAF, the photoconductive surface must be fabricated on a substrate that is much less than 25 μm of silicon. Recently, our group has been working on the development of ultra-thin silicon substrates (5-10 μm) that do not significantly scatter alpha particles.[28] Fabrication of an OET device on this etched silicon substrate is necessary for integration into the RARAF charged particle microbeams.

VI. CONCLUSION

The main contributions of this work are the integration of an optofluidic cell handling platform into the RARAF microbeam end station. The electrical conductivity of the particle-laden medium was optimized to give the maximum DEP force, and devices were fabricated at Columbia University's cleanroom. Experiments were performed to validate OET control of beads and cells, and to verify optofluidic manipulation before, during, and after UV microspot irradiation of cells. The addition of optofluidic manipulation at RARAF greatly improves the non-adherent cell handling capabilities of this facility. This is the first time that OET cell handling is successfully implemented in a biological microbeam.

ACKNOWLEDGMENTS

This research is supported through Grant No. P41 EB002033 to the Radiological Research Accelerator Facility from the National Institute of Biomedical Imaging and Bioengineering/National Institute of Health. The authors would like to acknowledge Dr. A. Ohta and Professor M. Wu, Berkeley University, for their helpful discussions and test sample. We also thank Dr. A. Asaithamby from D. Chen's group, University of Texas Southwestern, for providing HT1080 cells with GFP-tagged XRCC1.

[1] A. W. Bigelow, D. J. Brenner, G. Garty, and G. Randers-Pehrson, IEEE Trans. Plasma Sci. **36**(4), 1424–1431 (2008).
[2] C. Greubel, V. Hable, G. Drexler, A. Hauptner, S. Dietzel, H. Strickfaden, I. Baur, R. Krücken, T. Cremer, G. Dollinger, and A. Friedl, Radiat. Environ. Biophys. **47**(4), 423–429 (2008).
[3] H. Zhou, G. Randers-Pehrson, C. A. Waldren, D. Vannais, E. J. Hall, and T. K. Hei, Proc. Natl. Acad. Sci. U.S.A. **97**(5), 2099–2104 (2000).
[4] G. Randers-Pehrson, C. R. Geard, G. Johnson, C. D. Elliston, and D. J. Brenner, Radiat. Res. **156**(2), 210–214 (2001).
[5] A. Bigelow, G. Garty, T. Funayama, G. Randers-Pehrson, D. Brenner, and C. Geard, J. Radiat. Res. **50**(A), A21-A28 (2009).
[6] A. W. Bigelow, G. Randers-Pehrson, G. Garty, C. R. Geard, Y. Xu, A. D. Harken, G. W. Johnson, and D. J. Brenner, AIP Conf. Proc. **1336**(1), 351–355 (2011).
[7] G. Garty, M. Grad, B. K. Jones, Y. Xu, J. Xu, G. Randers-Pehrson, D. Attinger, and D. J. Brenner, Radiat. Prot. Dosim. **143**(2-4), 344–348 (2011).
[8] C. Chandsawangbhuwana, L. Z. Shi, Q. Zhu, M. C. Alliegro, and M. W. Berns, J. Biomed. Opt. **17**(1), 015001–015001 (2012).
[9] S. C. Santucci, D. Cojoc, H. Amenitsch, B. Marmiroli, B. Sartori, M. Burghammer, S. Schoeder, E. DiCola, M. Reynolds, and C. Riekel, Anal. Chem. **83**(12), 4863–4870 (2011).
[10] A. Ashkin, IEEE J. Sel. Top. Quantum Electron. **6**(6), 841–856 (2000).
[11] P. Y. Chiou, A. T. Ohta, and M. C. Wu, Nature (London) **436**(7049), 370–372 (2005).
[12] H. Hwang, and J.-K. Park, Lab Chip **11**(1), 33–47 (2011).
[13] A. T. Ohta, C. Pei-Yu, T. H. Han, J. C. Liao, U. Bhardwaj, E. R. B. McCabe, Y. Fuqu, S. Ren, and M. C. Wu, J. Microelectromech. Syst. **16**(3), 491–499 (2007).
[14] H. Hwang, Y.-J. Choi, W. Choi, S.-H. Kim, J. Jang, and J.-K. Park, Electrophoresis **29**(6), 1203–1212 (2008).
[15] P. J. Pauzauskie, A. Jamshidi, J. K. Valley, J. J. H. Satcher, and M. C. Wu, Appl. Phys. Lett. **95**(11), 113104 (2009).
[16] H. Shih-Hsun, L. Yen-Heng, and L. Gwo-Bin, J. Micromech. Microeng. **20**(4), 045026 (2010).
[17] D.-H. Lee, H. Hwang, and J.-K. Park, Appl. Phys. Lett. **95**(16), 164102 (2009).
[18] X. Zhu, H. Yi, and Z. Ni, Biomicrofluidics **4**(1), 013202–013214 (2010).
[19] X. Zhu, Z. Yin, and Z. Ni, Microfluid. Nanofluid. **12**(1), 529–544 (2012).
[20] H.-C. Chang and L. Y. Yeo, *Electrokinetically Driven Microfluidics and Nanofluidics* (Cambridge University Press, Cambridge, 2010).
[21] I. Ermolina and H. Morgan, J. Colloid Interface Sci. **285**(1), 419–428 (2005).
[22] A. C. Ruege and R. M. Reano, Opt. Express **17**(6), 4295–4305 (2009).
[23] J. K. Valley, A. Jamshidi, A. T. Ohta, H. Hsan-Yin, and M. C. Wu, J.Microelectromech. Syst. **17**(2), 342–350 (2008).
[24] A. Asaithamby and D. J. Chen, Mutat. Res. **711** (1–2), 87–99 (2011).
[25] R. R. Anderson and J. A. Parrish, Science **220**(4596), 524–527 (1983).
[26] A. N. Hellman, K. R. Rau, H. H. Yoon, and V. Venugopalan, J. Biophotonics **1**(1), 24–35 (2008).
[27] K. König, J. Microsc. **200**(2), 83–104 (2000).
[28] M. Grad, A. Harken, G. Randers-Pehrson, D. Attinger, and D. J. Brenner, J. Instrum. **7**(12), P12001 (2012).
[29] See Supplementary material at http://dx.doi.org/10.1063/1.4774043 for MATLAB code.